Letter

Giant orbital polarization of Ni^{2+} in a square planar environment

Prithwijit Mandal,[1,*] Ranjan Kumar Patel,[1,*] Dibyata Rout,[2] Rajdeep Banerjee,[3] Rabindranath Bag,[2] Koushik Karmakar,[2] Awadhesh Narayan,[3] John W. Freeland,[4] Surjeet Singh,[2] and Srimanta Middey[1,†]

[1]*Department of Physics, Indian Institute of Science, Bengaluru 560012, India*

[2]*Department of Physics, Indian Institute of Science Education and Research, Pune, Maharashtra 411008, India*

[3]*Solid State and Structural Chemistry Unit, Indian Institute of Science, Bengaluru 560012, India*

[4]*Advanced Photon Source, Argonne National Laboratory, Argonne, Illinois 60439, USA*

(Received 28 September 2020; revised 2 December 2020; accepted 19 January 2021; published 17 February 2021)

Finding large orbital polarization in Ni-based oxides has become a topic of paramount interest in recent years due to the prospect of finding superconductivity. In this work, we investigate the electronic structure of single-crystalline samples of Sr_2CuO_3 and Ni-doped Sr_2CuO_3 containing Cu/NiO_4 square planar units. Our polarization-dependent x-ray absorption spectroscopy experiments reveal extremely large orbital polarization ($\sim$63%) for Ni^{2+}. Cluster calculations and *ab initio* calculations find that the giant orbital polarization arises due to the low-spin ($S = 0$) configuration with two holes in the Ni $3d_{x^2-y^2}$ orbital, contrary to the expected high-spin ($S = 1$) state from Hund's first rule.

DOI: 10.1103/PhysRevB.103.L060504

Transition metal oxides (TMOs) exhibit a variety of tunable electronic, magnetic, and topological phases due to the strong intercoupling among charge, spin, lattice, and orbital degrees of freedom [1–3]. In particular, large orbital polarization plays a decisive role in giving rise to several interesting phenomena in various TMOs, including charge density wave instabilities and metal-insulator transitions in titanates, vanadates, and nickelates [4–7]; emergent magnetic phases in titanates and manganites [8–10]; and high-T_c superconductivity in cuprates [2,11,12]. Designing new materials to achieve large orbital polarization has become a recurring theme in the contemporary condensed-matter physics [13–19]. After the theoretical prediction of achieving a cuprate like Fermi surface in the three-dimensional compound $LaNiO_3$ through orbital engineering [20–22], various types of artificial structures of the $RENiO_3$ (*RE*: rare-earth elements) family have been extensively investigated [7,13–15]. However, the observed orbital polarization in an octahedral symmetry is low ($\leqslant$25%), and superconductivity remains elusive there. The recent finding of superconductivity in Sr-doped $NdNiO_2$ with Ni in the square planar coordinate is, therefore, a monumental development [23] and strongly implies that the local structure [O_h vs. D_{4h} in Fig. 1(a)] and the resultant spin and orbital structures of Ni ions play the central role.

This discovery has led to a large number of works within a short span of time to understand the origin and nature of the superconducting phase [26–39]. While the parent members of the superconducting nickelate and cuprate families are isoelectronic (d^9), several key differences have been noted: unlike the antiferromagnetic insulating phase of cuprates, $NdNiO_2$ is weakly conducting and nonmagnetic [23], and the superconducting T_c is much smaller than that of the analogous hole-doped $CaCuO_2$ [27,28,40]. There is also an ongoing strong debate about the location of doped holes and the nature of the Ni spin state: d^8 and $S = 1$ vs d^8 and $S = 0$ vs the Zhang-Rice singlet $d^9\underline{L}$ ($\underline{L}$ denotes a hole in the O $2p$ state) [32,33,35–38,41]. However, the actual scenario is unknown due to a very limited amount of experimental work done in this direction. This prompts us to probe other compounds containing both Cu and Ni in a fourfold-coordinated environment of oxygen.

Here, we focus on Sr_2CuO_3 (SCO), where square planar CuO_4 polyhedral units form linear chains along the b axis [Fig. 1(b)] [42]. This quasi-one-dimensional system undergoes antiferromagnetic ordering around 5 K [43] and exhibits several intriguing phenomena, including spin-charge separation [44], spin-orbital separation [45], spin Seebeck effect [46], and superconductivity by incorporating excess oxygen [47]. Electronic structure investigations have revealed that Cu in SCO has an extremely small value for the charge transfer energy Δ [48–51]. It implies that the ground state of Cu^{2+} in SCO consists of a linear combination of d^9 and dominant $d^{10}\underline{L}$ configurations, in contrast to the pure d^9 state expected from an ionic picture [52]. Interestingly, one can replace a small fraction of Cu in SCO with Ni without modifying the structure [53], providing us a unique platform to compare the electronic structure of Cu and Ni within a square planar environment.

In this paper, we investigate the electronic and magnetic structure of SCO and $Sr_2Cu_{0.9}Ni_{0.1}O_3$ (SCNO) single crystals by magnetic measurement, synchrotron-based x-ray linear dichroism (XLD) measurements, density functional theory (DFT), and cluster calculations. We report extremely large orbital polarization of Ni in the $Sr_2Cu_{0.9}Ni_{0.1}O_3$ single crystal, which arises due to the low-spin ($S = 0$) configuration with completely unoccupied $3d_{x^2-y^2}$ orbitals of Ni^{2+}. Ni doping of SCO also enhances the contribution of the d^9 configuration in the ground state of Cu^{2+}.

*These authors contributed equally to this work.

†Corresponding author: smiddey@iisc.ac.in

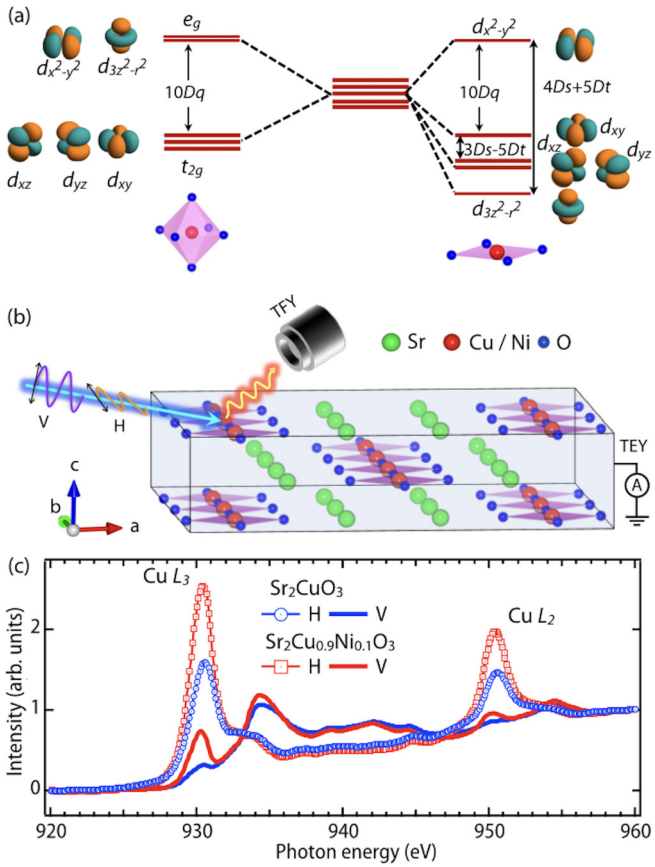

FIG. 1. (a) Energy level splitting of transition metal d orbitals due to point-charge (Coulomb) contributions under octahedral (O_h) and square planar (D_{4h}) environments [24]. The ordering of these levels can be modified in solids due to the hybridization between transition metal d and oxygen p states [25]. (b) Crystal structure of $Sr_2(Cu,Ni)O_3$ and experimental arrangement for XAS experiment with out-of-plane (V) and in-plane (H) polarized rays. TFY and TEY denote total fluorescence yield and total electron yield, respectively. (c) Cu $L_{3,2}$-edge XAS recorded in the bulk-sensitive TFY mode with V and H x rays.

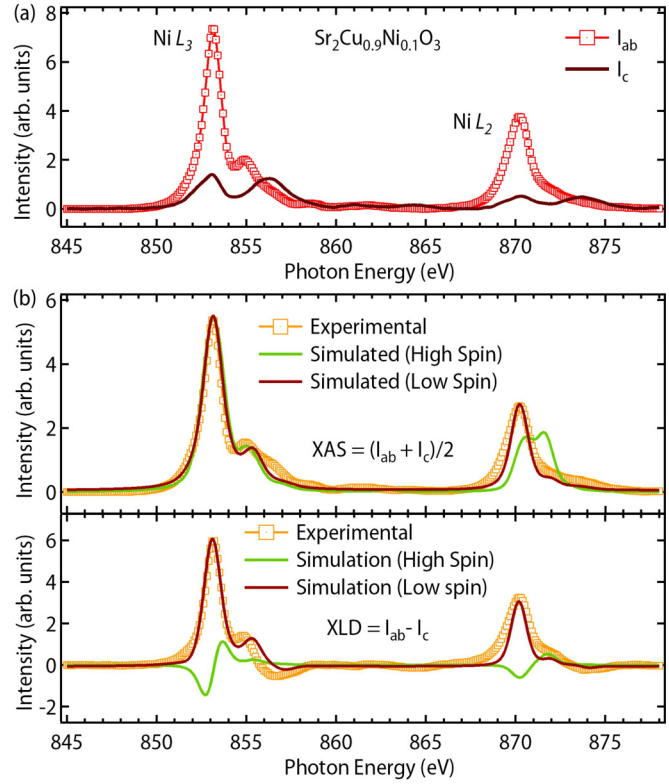

FIG. 2. (a) Ni L_3 and L_2 XAS (TFY mode) for $Sr_2Cu_{0.9}Ni_{0.1}O_3$, recorded with V and H polarizations. These spectra have been plotted after background subtraction (see the Supplemental Material (SM) [57]) (b) Top (bottom): Experimentally observed isotropic XAS (XLD) and simulated XAS (XLD) spectra. The simulation is done for Ni^{2+} with $S = 1$ and $S = 0$ configurations.

Single crystals of SCO and SCNO were grown using the traveling solvent floating zone technique [54]. All the experiments reported here were carried out on as grown crystals. The magnetic susceptibility was measured using a physical property measurement system (Quantum Design). X-ray absorption spectra (XAS) with vertically (V) and horizontally (H) polarized x rays were recorded at room temperature at the 4-ID-C beamline of the Advanced Photon Source.

We first discuss the results of the polarization-dependent XAS experiment on Cu $L_{3,2}$ edges [11,12,55,56]. XAS (I_{ab}) of SCO [Fig. 1(c)] recorded with in-plane (H) polarized light consists of sharp peaks around 930.5 and 950.5 eV, which are associated with the transition from the spin-orbit split Cu $2p_{3/2}$ and Cu $2p_{1/2}$ core levels, respectively, and the final state configuration is $2\underline{p}3d^{10}$ ($2\underline{p}$ denotes a core hole in Cu $2p$ states). The much lower intensity of these peaks in XAS (I_c) with the out-of-plane (V) polarization signifies that the upper Hubbard band is predominately contributed by Cu $d_{x^2-y^2}$ orbitals. The features around 934 and 954.5 eV, which are much stronger for the out-of-plane polarization, are related to the transitions into Cu $3d_{3z^2-r^2}$ derived states, which become partially unoccupied due to the hybridization with Cu $4s$ states [56]. Upon Ni doping, the intensity of the white line increases significantly for both polarizations, though the line shape remains unchanged [Fig. 1(c)].

Results of polarization-dependent XAS experiments at the Ni $L_{3,2}$ edges of SCNO at 300 K are shown in Fig. 2(a). The two intense peaks around 853 and 870 eV in the spectrum, recorded with the in-plane polarization (I_{ab}), correspond to the transitions from Ni $2p_{3/2}$ and Ni $2p_{1/2}$ core levels, respectively. I_c, recorded with the out-plane polarization, shows significantly low intensity, indicating that the holes predominantly occupy the $d_{x^2-y^2}$ bands. The peaks around 856 and 874 eV show higher intensity in I_c than I_{ab}. These features are related to the hybridization of Ni $3d_{3z^2-r^2}$ and Ni $4s$ states. Since the experimental realization of large orbital polarization (OP) in Ni-based oxides, with important implications for superconductivity, has been a topic of paramount interest [15–18], we further evaluate the OP of Ni in the present case. According to the sum rule of linear polarization [15–19,58], the ratio of holes in $d_{3z^2-r^2}$ and $d_{x^2-y^2}$ is defined as $X = \frac{h_{3z^2-r^2}}{h_{x^2-y^2}} = \frac{3I'_c}{4I'_{ab}-I'_c}$ with $I'_{ab,c} = \int I_{ab,c}(E)dE$. By this definition, $X = 1$ corresponds to an equal hole population in $d_{3z^2-r^2}$ and $d_{x^2-y^2}$ orbitals, and $X = 0$ signifies 100%

TABLE I. Comparison of the hole ratio for Ni $3d_{x^2-y^2}$ and Ni $3d_{3z^2-r^2}$ orbitals and percentage of holes in Ni $3d_{x^2-y^2}$ for $Sr_2Cu_{0.9}Ni_{0.1}O_3$ with the literature.

System	X	Percentage of holes in Ni $d_{x^2-y^2}$	Ref.
$SrCuO_2/LaNiO_3$	0.7	59	[16]
$LaTiO_3/LaNiO_3/LaAlO_3$	0.55	65	[17]
$La_4Ni_3O_8$	0.4–0.5	67–71	[18]
$Sr_2Cu_{0.9}Ni_{0.1}O_3$	0.23	81	present work

$d_{x^2-y^2}$ character of holes. We have obtained $X \approx 0.23$ (also see the SM [57]) in the present case. This implies 81% of the holes occupy the Ni $3d_{x^2-y^2}$ orbital, which is the highest among the existing literature of Ni-based complex oxides (see Table I).

The orbital polarization P is defined in the literature [15] in terms of the electronic occupation as $P = \frac{n_{3z^2-r^2}-n_{x^2-y^2}}{n_{3z^2-r^2}+n_{x^2-y^2}} = (\frac{4}{n'}-1)\frac{(1-X)}{(1+X)}$, where $n_{x^2-y^2} = 2 - h_{x^2-y^2}$ and $n_{3z^2-r^2} = 2 - h_{3z^2-r^2}$ are the numbers of electrons in $d_{x^2-y^2}$ and $d_{3z^2-r^2}$ orbitals, respectively. It is important to note that the value of n' $(= n_{x^2-y^2} + n_{3z^2-r^2})$ cannot be determined unambiguously for many compounds due to the presence of charge transfer from O $2p$ to Ni $3d$ orbitals [15,59]. In the present case, $n' \sim 2$ as the ground state wave function is dominantly contributed by the d^8 configuration. We have obtained $P \approx 63\%$ for SCNO, which is also larger compared to all existing literatures on Ni-based complex oxides (Table I) [7,15–18,60].

In order to understand the origin of this large orbital polarization, we have calculated XAS $[(I_{ab} + I_c)/2]$ and XLD $(I_{ab} - I_c)$ of Ni $L_{3,2}$ edges considering a NiO_4 cluster with D_{4h} symmetry and the Ni^{2+} ionic configuration using the CTM4XAS [61] and QUANTY [62] programs that incorporate ligand field multiplet theory. We performed simulations for the high-spin ($S = 1$) configuration [63,64] (all parameters, used for the simulations are listed in Ref. [65]). Clearly, neither the simulated XAS nor the XLD [Fig. 2(b)] matches the corresponding experimental spectrum. In particular, the experimentally observed L_2-edge XAS shows only one peak around 870 eV, whereas the simulated spectra show two peaks. The shape of the simulated XLD is completely different from the experimental data. We have also simulated XAS and XLD for the low-spin configuration ($S = 0$) by adjusting the crystal field parameters [65], which ensures the expected crystal field splitting $d_{3z^2-r^2} < d_{xz/yz} < d_{xy} < d_{x^2-y^2}$ for a square planar environment [24]. The excellent matching [Fig. 2(b)] between the experimentally observed and simulated spectra with the low-spin configuration establishes Ni^{2+} is in the $S = 0$ state in the square planar environment.

Simulated spectra with $U > \Delta$ also do not match the experimental observation (see the SM for XAS and XLD simulations for different values of Δ considering $U = 7$ eV [57]). We estimate $\Delta \sim 7$–9 eV in the present case, implying that, electronically, NiO_4 belongs near the boundary between the Mott-Hubbard insulating region and the charge transfer insulating region of the Zaanen-Sawatzky-Allen phase diagram [26,41,48]. Due to the large Δ, Ni d is less hybridized with O p compared to the Cu d-O p hybridization. Thus, the replacement of a fraction of Cu by Ni pushes holes from O p towards Cu d around the dopant Ni. This enhances the relative contribution of the d^9 configuration, resulting in the observed strong increase in the white line intensity in Cu XAS upon Ni doping [Fig. 1(c)].

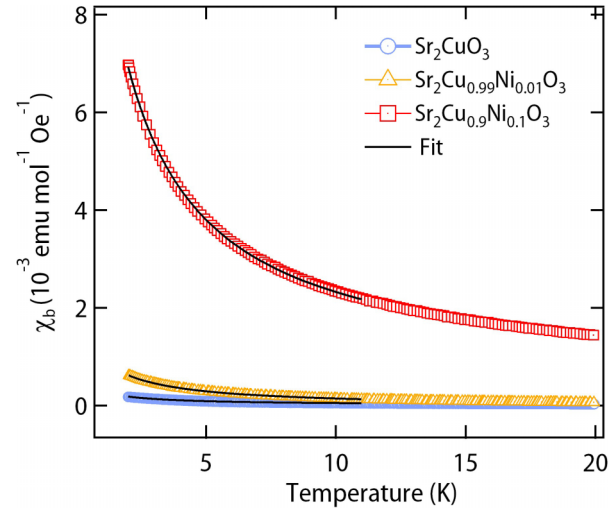

FIG. 3. Temperature dependence of magnetic susceptibility χ and fitting by the Curie-Weiss law. For details, see Refs. [53,66–69]. The data for 1% Ni-doped SCO sample were adapted from Ref. [53].

The increase in the d^9 component of Cu due to the presence of nonmagnetic Ni^{2+} is also evident in bulk magnetic measurements. Low-temperature magnetic susceptibility χ plots of pristine and 1% and 10% Ni-doped SCO samples are shown in Fig. 3. As expected, χ of SCO is very small due to the antiferromagnetic coupling between the neighboring Cu spins. Upon Ni doping, the -O-Cu-O-Cu-O- chain breaks into finite-length segments due to an effective spin 0 on the Ni ion. The number of segments thus produced is $p + 1 \sim p$ for large p, where p is the concentration of Ni. Assuming a statistically random distribution of Ni ions over the chain length, it is reasonable to consider that one half of the chain segments will have an odd number of Cu spins, with an even number for the remaining segments. Since Cu spins are antiferromagnetically paired, the net moment on the even-length segments tends to zero at sufficiently low temperatures [70]. In contrast, the odd-length segments retain an uncompensated Cu spin, which results in an enhancement in the magnetic response of Ni-doped samples, as seen in Fig. 3. A very weak Curie tail in the pristine sample can be attributed to the presence of intrinsic defects. We fitted the low-temperature susceptibility of our samples using the Curie-Weiss (CW) law: $\chi = \chi_0 + C/(T - \theta_{CW})$, where χ_0 is the temperature-independent contribution arising due to Van Vleck paramagnetism and core diamagnetism, C is the Curie constant, and θ_{CW} is the Weiss temperature. The best-fit parameters for the three samples are tabulated in the SM [57]. From C, μ_{eff} $(= \sqrt{8C})$ for the two Ni-doped samples ($p = 0.01$ and 0.1) turned out to be $\sim 0.12\mu_B$ and $\sim 0.38\mu_B$ per formula unit, respectively. The average effective moment on the odd-length segments $[=\sqrt{8C/(0.5p)}]$ turns out to be $1.74\mu_B$ and $1.70\mu_B$, respectively, for the two samples. These

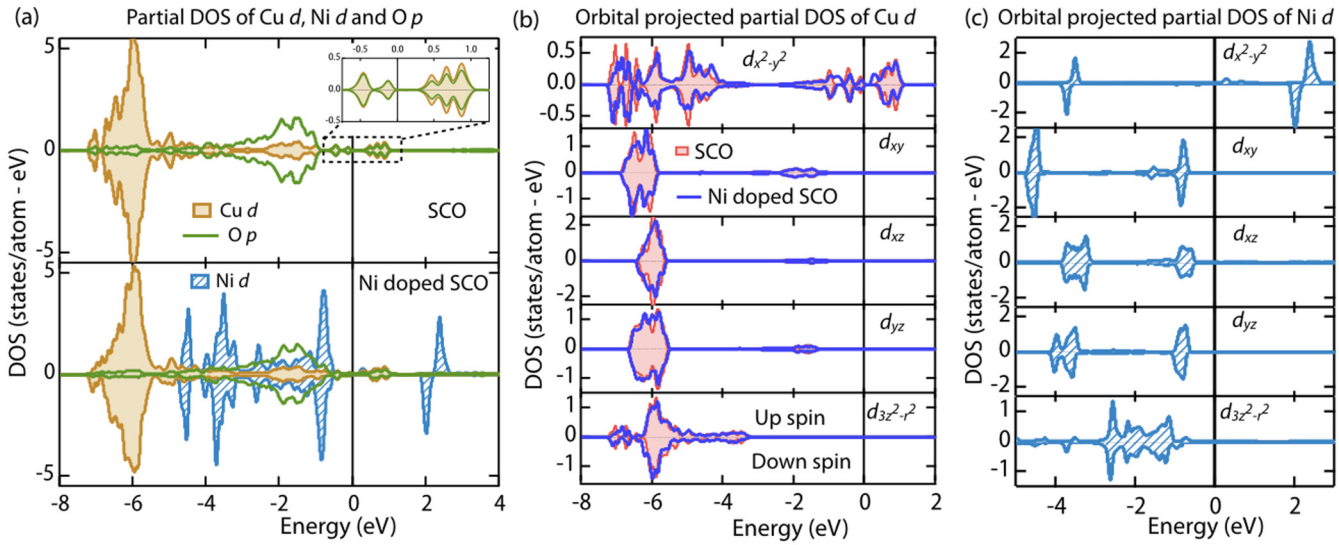

FIG. 4. Orbital projected partial density of states: (a) comparison of DOS of Cu d and O p states of undoped SCO (top panel) with DOS of Cu d, O p, and Ni d states of Ni-doped SCO (bottom panel), (b) comparison of different Cu d states of doped (line) and undoped (line + shading) SCO, and (c) different d-orbital projected DOSs of Ni in doped SCO. The vertical line at zero energy indicates the Fermi level.

values are close to an effective moment of $\sim 1.73\mu_B$ expected for an $S = 1/2$ (d^9) system, confirming our conclusion for the Cu XAS measurement.

To obtain a microscopic understanding of our experimental observations, we have carried out first-principles DFT calculations for Sr_2CuO_3 and $Sr_2Cu_{0.875}Ni_{0.125}O_3$ (details are in the SM [57]). The calculated orbital projected densities of states (DOS) are shown in Fig. 4. In contrast to the transition metal oxides with positive Δ, the bonding states of SCO are primarily contributed by Cu d orbitals due to negative Δ [25]. The Cu d_{xy}, d_{xz}, d_{yz}, and $d_{3z^2-r^2}$ bonding states are spread around 6 eV below the Fermi level [Fig. 4(b)]. The valence band and conduction band edges of undoped SCO come predominantly from O p states [inset of Fig. 4(a)], as expected for a covalent insulator [51]. The $d_{x^2-y^2}$ antibonding states are partially unoccupied, in line with our XAS results. We find that the magnetic moment of Cu is close to $0.19\mu_B$. The slight overestimation of this moment, compared to the experimentally observed moment ($\sim 0.06\mu_B$) [43] is likely to be related to the presence of the quantum fluctuation effects in SCO, which are not accounted for in a mean-field approach like DFT. The much smaller moment, compared to the expected moment of $1.73\mu_B$ for a pure d^9 ($S = 1/2$) configuration, again signifies that the ground state of Cu^{2+} in SCO is predominantly the $d^{10}\underline{L}$ configuration with a small admixture with d^9.

Our DFT calculations of 12.5% Ni-doped SCO obtain Cu magnetic moments ranging from $0.13\mu_B$ to $0.24\mu_B$ and a net moment of $\sim 0.13\mu_B$ per formula unit. This also supports our observation about the increase of white line intensity of Cu XAS [Fig. 1(c)] and magnetic measurement i.e., the enhancement of the d^9 configuration of Cu upon Ni doping. For Ni-doped SCO, the contribution arising from different Ni d orbitals is shown in Fig. 4(c) [also see the bottom panel of Fig. 4(a)]. The antibonding states of the Ni $d_{x^2-y^2}$ orbital are completely unoccupied, while all other Ni $3d$ states are completely filled. This low-spin ($S = 0$) configuration of Ni with holes in the $d_{x^2-y^2}$ orbital is in excellent agreement with our experimental observations.

To summarize, our element-sensitive x-ray absorption spectroscopy experiments with linearly polarized light for $Sr_2Cu_{0.9}Ni_{0.1}O_3$ have found that 81% of holes of Ni^{2+} sites occupy the $d_{x^2-y^2}$ orbital. Ni doping in Sr_2CuO_3 also results in hole transfer from O p to Cu d orbitals. Cluster calculations have revealed that the observed giant orbital polarization arises due to the low-spin ($S = 0$) configuration of Ni^{2+}. This nonmagnetic state of Ni^{2+} has been further corroborated by *ab initio* theory.

Finally, we also note that our investigated system has several parallels with the recently discovered superconducting nickelates. Ionically, Sr doping in $NdNi^{+1}O_2$ would result in an equivalent amount of Ni with a +2 oxidation state. Our system comprises NiO_4 units forming one-dimensional chains, while the superconducting nickelates have a two-dimensional NiO_2 plane. It is expected that the increase in the dimensionality of the system would further enhance Δ [71], and therefore, our conclusions about the electronic structure of Ni^{2+} should also hold for nickelate superconductors.

Recently, a preprint appeared about the XAS and resonant inelastic x-ray scattering study of $Nd_{1-x}Sr_xNiO_2$ [72] which also reports that the doped holes are in the Ni $3d_{x^2-y^2}$ orbital with a d^8 $S = 0$ state.

S.M. thanks T. Das and H. R. Krishnamurthy for discussions. S.M. acknowledges financial support from a SERB Early Career Research Award (Grant No. ECR/2018/001512) and the MHRD STARS 156/2019 project for research funding. S.M. also thanks the Department of Science and Technology, India (Grant No. SR/NM/Z-07/2015), for the financial support to conduct the synchrotron experiment at the Advanced Photon Source and Jawaharlal Nehru Centre for Advanced Scientific Research (JNCASR) for managing the project. This research used resources of the Advanced Photon Source, a U.S. Department of Energy Office of Science User

Facility operated by Argonne National Laboratory under Contract No. DE-AC02-06CH11357. A.N. acknowledges support from the start-up grant (Grant No. SG/MHRD-19-0001) of the Indian Institute of Science and DST-SERB (project number SRG/2020/000153). SS thanks MHRD STARS for financial support under STARS/APR2019/358.

[1] M. Imada, A. Fujimori, and Y. Tokura, Rev. Mod. Phys. **70**, 1039 (1998).
[2] B. Keimer, S. A. Kivelson, M. R. Norman, S. Uchida, and J. Zaanen, Nature (London) **518**, 179 (2015).
[3] Y. Tokura, M. Kawasaki, and N. Nagaosa, Nat. Phys. **13**, 1056 (2017).
[4] C. F. Chang, T. C. Koethe, Z. Hu, J. Weinen, S. Agrestini, L. Zhao, J. Gegner, H. Ott, G. Panaccione, H. Wu *et al.*, Phys. Rev. X **8**, 021004 (2018).
[5] M. W. Haverkort, Z. Hu, A. Tanaka, W. Reichelt, S. V. Streltsov, M. A. Korotin, V. I. Anisimov, H. H. Hsieh, H.-J. Lin, C. T. Chen, D. I. Khomskii, and L. H. Tjeng, Phys. Rev. Lett. **95**, 196404 (2005).
[6] N. B. Aetukuri, A. X. Gray, M. Drouard, M. Cossale, L. Gao, A. H. Reid, R. Kukreja, H. Ohldag, C. A. Jenkins, E. Arenholz, K. P. Roche, H. A. Dürr, M. G. Samant, and S. S. P. Parkin, Nat. Phys. **9**, 661 (2013).
[7] S. Middey, J. Chakhalian, P. Mahadevan, J. W. Freeland, A. J. Millis, and D. D. Sarma, Annu. Rev. Mater. Res. **46**, 305 (2016).
[8] J. Garcia-Barriocanal, J. Cezar, F. Bruno, P. Thakur, N. Brookes, C. Utfeld, A. Rivera-Calzada, S. Giblin, J. Taylor, J. Duffy, S. Dugdale, T. Nakamura, K. Kodama, C. Leon, S. Okamoto, and J. Santamaria, Nat. Commun. **1**, 82 (2010).
[9] P. Yu, J.-S. Lee, S. Okamoto, M. D. Rossell, M. Huijben, C.-H. Yang, Q. He, J. X. Zhang, S. Y. Yang, M. J. Lee, Q. M. Ramasse, R. Erni, Y.-H. Chu, D. A. Arena, C.-C. Kao, L. W. Martin, and R. Ramesh, Phys. Rev. Lett. **105**, 027201 (2010).
[10] M. Salluzzo, S. Gariglio, D. Stornaiuolo, V. Sessi, S. Rusponi, C. Piamonteze, G. M. De Luca, M. Minola, D. Marré, A. Gadaleta, H. Brune, F. Nolting, N. B. Brookes, and G. Ghiringhelli, Phys. Rev. Lett. **111**, 087204 (2013).
[11] N. Nücker, E. Pellegrin, P. Schweiss, J. Fink, S. L. Molodtsov, C. T. Simmons, G. Kaindl, W. Frentrup, A. Erb, and G. Müller-Vogt, Phys. Rev. B **51**, 8529 (1995).
[12] J. Chakhalian, J. W. Freeland, H.-U. Habermeier, G. Cristiani, G. Khaliullin, M. van Veenendaal, and B. Keimer, Science **318**, 1114 (2007).
[13] J. W. Freeland, J. Liu, M. Kareev, B. Gray, J. W. Kim, P. J. Ryan, R. Pentcheva, and J. Chakhalian, Europhys. Lett. **96**, 57004 (2011).
[14] E. Benckiser, M. W. Haverkort, S. Brck, E. Goering, S. Macke, A. Frañó, X. Yang, O. K. Andersen, G. Cristiani, H.-U. Habermeier, A. V. Boris, I. Zegkinoglou, P. Wochner, H.-J. Kim, V. Hinkov, and B. Keimer, Nat. Mater. **10**, 189 (2011).
[15] M. Wu, E. Benckiser, M. W. Haverkort, A. Frano, Y. Lu, U. Nwankwo, S. Brück, P. Audehm, E. Goering, S. Macke, V. Hinkov, P. Wochner, G. Christiani, S. Heinze, G. Logvenov, H.-U. Habermeier, and B. Keimer, Phys. Rev. B **88**, 125124 (2013).
[16] Z. Liao, E. Skoropata, J. W. Freeland, E.-J. Guo, R. Desautels, X. Gao, C. Sohn, A. Rastogi, T. Z. Ward, T. Zou, T. Charlton, M. R. Fitzsimmons, and H. N. Lee, Nat. Commun. **10**, 589 (2019).
[17] A. S. Disa, D. P. Kumah, A. Malashevich, H. Chen, D. A. Arena, E. D. Specht, S. Ismail-Beigi, F. J. Walker, and C. H. Ahn, Phys. Rev. Lett. **114**, 026801 (2015).
[18] J. Zhang, A. S. Botana, J. W. Freeland, D. Phelan, H. Zheng, V. Pardo, M. R. Norman, and J. F. Mitchell, Nat. Phys. **13**, 864 (2017).
[19] S. Lee, A. T. Lee, A. B. Georgescu, G. Fabbris, M.-G. Han, Y. Zhu, J. W. Freeland, A. S. Disa, Y. Jia, M. P. M. Dean, F. J. Walker, S. Ismail-Beigi, and C. H. Ahn, Phys. Rev. Lett. **123**, 117201 (2019).
[20] V. I. Anisimov, D. Bukhvalov, and T. M. Rice, Phys. Rev. B **59**, 7901 (1999).
[21] J. Chaloupka and G. Khaliullin, Phys. Rev. Lett. **100**, 016404 (2008).
[22] P. Hansmann, X. Yang, A. Toschi, G. Khaliullin, O. K. Andersen, and K. Held, Phys. Rev. Lett. **103**, 016401 (2009).
[23] D. Li, K. Lee, B. Y. Wang, M. Osada, S. Crossley, H. R. Lee, Y. Cui, Y. Hikita, and H. Y. Hwang, Nature (London) **572**, 624 (2019).
[24] M. M. Sala, V. Bisogni, C. Aruta, G. Balestrino, H. Berger, N. B. Brookes, G. M. de Luca, D. D. Castro, M. Grioni, M. Guarise, P. G. Medaglia, F. M. Granozio, M. Minola, P. Perna, M. Radovic, M. Salluzzo, T. Schmitt, K. J. Zhou, L. Braicovich, and G. Ghiringhelli, New J. Phys. **13**, 043026 (2011).
[25] A. V. Ushakov, S. V. Streltsov, and D. I. Khomskii, J. Phys.: Condens. Matter **23**, 445601 (2011).
[26] M. Hepting, D. Li, C. J. Jia, H. Lu, E. Paris, Y. Tseng, X. Feng, M. Osada, E. Been, Y. Hikita *et al.*, Nat. Mater. **19**, 381 (2020).
[27] D. Li, B. Y. Wang, K. Lee, S. P. Harvey, M. Osada, B. H. Goodge, L. F. Kourkoutis, and H. Y. Hwang, Phys. Rev. Lett. **125**, 027001 (2020).
[28] S. Zeng, C. S. Tang, X. Yin, C. Li, Z. Huang, J. Hu, W. Liu, G. J. Omar, H. Jani, Z. S. Lim, K. Han, D. Wan, P. Yang, S. J. Pennycook, A. T.-S. Wee, and A. Ariando, Phys. Rev. Lett. **125**, 147003 (2020).
[29] A. S. Botana and M. R. Norman, Phys. Rev. X **10**, 011024 (2020).
[30] F. Lechermann, Phys. Rev. B **101**, 081110(R) (2020).
[31] P. Jiang, L. Si, Z. Liao, and Z. Zhong, Phys. Rev. B **100**, 201106(R) (2019).
[32] J. Karp, A. S. Botana, M. R. Norman, H. Park, M. Zingl, and A. Millis, Phys. Rev. X **10**, 021061 (2020).
[33] L.-H. Hu and C. Wu, Phys. Rev. Research **1**, 032046(R) (2019).
[34] P. Adhikary, S. Bandyopadhyay, T. Das, I. Dasgupta, and T. Saha-Dasgupta, Phys. Rev. B **102**, 100501(R) (2020).
[35] M. Jiang, M. Berciu, and G. A. Sawatzky, Phys. Rev. Lett. **124**, 207004 (2020).
[36] Y.-H. Zhang and A. Vishwanath, Phys. Rev. Research **2**, 023112 (2020).
[37] H. Zhang, L. Jin, S. Wang, B. Xi, X. Shi, F. Ye, and J.-W. Mei, Phys. Rev. Research **2**, 013214 (2020).

[38] Z.-J. Lang, R. Jiang, and W. Ku, arXiv:2005.00022.

[39] J. Krishna, H. LaBollita, A. O. Fumega, V. Pardo, and A. S. Botana, Phys. Rev. B **102**, 224506 (2020).

[40] M. Azuma, Z. Hiroi, M. Takano, Y. Bando, and Y. Takeda, Nature (London) **356**, 775 (1992).

[41] B. H. Goodge, D. Li, M. Osada, B. Y. Wang, K. Lee, G. A. Sawatzky, H. Y. Hwang, and L. F. Kourkoutis, PNAS **118**, e2007683118 (2021).

[42] N. Motoyama, H. Eisaki, and S. Uchida, Phys. Rev. Lett. **76**, 3212 (1996).

[43] K. M. Kojima, Y. Fudamoto, M. Larkin, G. M. Luke, J. Merrin, B. Nachumi, Y. J. Uemura, N. Motoyama, H. Eisaki, S. Uchida, K. Yamada, Y. Endoh, S. Hosoya, B. J. Sternlieb, and G. Shirane, Phys. Rev. Lett. **78**, 1787 (1997).

[44] R. Neudert, M. Knupfer, M. S. Golden, J. Fink, W. Stephan, K. Penc, N. Motoyama, H. Eisaki, and S. Uchida, Phys. Rev. Lett. **81**, 657 (1998).

[45] J. Schlappa, K. Wohlfeld, K. J. Zhou, M. Mourigal, M. W. Haverkort, V. N. Strocov, L. Hozoi, C. Monney, S. Nishimoto, S. Singh *et al.*, Nature **485**, 82 (2012).

[46] D. Hirobe, M. Sato, T. Kawamata, Y. Shiomi, K.-i. Uchida, R. Iguchi, Y. Koike, S. Maekawa, and E. Saitoh, Nat. Phys. **13**, 30 (2017).

[47] Z. Hiroi, M. Takano, M. Azuma, and Y. Takeda, Nature (London) **364**, 315 (1993).

[48] J. Zaanen, G. A. Sawatzky, and J. W. Allen, Phys. Rev. Lett. **55**, 418 (1985).

[49] S. Nimkar, D. D. Sarma, H. R. Krishnamurthy, and S. Ramasesha, Phys. Rev. B **48**, 7355 (1993).

[50] K. Maiti, D. D. Sarma, T. Mizokawa, and A. Fujimori, Europhys. Lett. **37**, 359 (1997).

[51] K. Maiti, D. D. Sarma, T. Mizokawa, and A. Fujimori, Phys. Rev. B **57**, 1572 (1998).

[52] A. C. Walters, T. G. Perring, J.-S. Caux, A. T. Savici, G. D. Gu, C.-C. Lee, W. Ku, and I. A. Zaliznyak, Nat. Phys. **5**, 867 (2009).

[53] K. Karmakar and S. Singh, Phys. Rev. B **91**, 224401 (2015).

[54] K. Karmakar, R. Bag, and S. Singh, Cryst. Growth Des. **15**, 4843 (2015).

[55] M. Knupfer, R. Neudert, M. Kielwein, S. Haffner, M. S. Golden, J. Fink, C. Kim, Z.-X. Shen, M. Merz, N. Nücker, S. Schuppler, N. Motoyama, H. Eisaki, S. Uchida, Z. Hu, M. Domke, and G. Kaindl, Phys. Rev. B **55**, R7291 (1997).

[56] R. Neudert, S.-L. Drechsler, J. Málek, H. Rosner, M. Kielwein, Z. Hu, M. Knupfer, M. S. Golden, J. Fink, N. Nücker, M. Merz, S. Schuppler, N. Motoyama, H. Eisaki, S. Uchida, M. Domke, and G. Kaindl, Phys. Rev. B **62**, 10752 (2000).

[57] See Supplemental Material at http://link.aps.org/supplemental/10.1103/PhysRevB.103.L060504 for multiplet cluster calculations, extraction of the orbital polarization, analysis of magnetic susceptibilities, and details of DFT calculations, which include Ref. [73–77].

[58] G. Van der Laan, J. Phys. Soc. Jpn. **63**, 2393 (1994).

[59] O. E. Peil, M. Ferrero, and A. Georges, Phys. Rev. B **90**, 045128 (2014).

[60] S. Middey, D. Meyers, D. Doennig, M. Kareev, X. Liu, Y. Cao, Z. Yang, J. Shi, L. Gu, P. J. Ryan, R. Pentcheva, J. W. Freeland, and J. Chakhalian, Phys. Rev. Lett. **116**, 056801 (2016).

[61] E. Stavitski and F. M. De Groot, Micron **41**, 687 (2010).

[62] M. W. Haverkort, M. Zwierzycki, and O. K. Andersen, Phys. Rev. B **85**, 165113 (2012). Also see http://www.quanty.org/.

[63] Y. Utz, F. Hammerath, R. Kraus, T. Ritschel, J. Geck, L. Hozoi, J. van den Brink, A. Mohan, C. Hess, K. Karmakar, S. Singh, D. Bounoua, R. Saint-Martin, L. Pinsard-Gaudart, A. Revcolevschi, B. Büchner, and H.-J. Grafe, Phys. Rev. B **96**, 115135 (2017).

[64] G. van der Laan, B. T. Thole, G. A. Sawatzky, and M. Verdaguer, Phys. Rev. B **37**, 6587 (1988).

[65] $\Delta = 9$ eV, $U_{dd} = 7$ eV, $U_{pd} = 9$ eV were used in cluster calculations. The hopping parameters, related to d_{z^2}, $d_{x^2-y^2}$, d_{xy}, and d_{xz}/d_{yz} orbitals, were chosen to be 2.0, 2.0, 1.0, and 1.0 eV, respectively. For the high-spin ($S = 1$) configuration, the crystal field parameters for D_{4h} symmetry were chosen to be $Dq = 0.235$ eV, $Ds = 0.1$ eV, $Dt = 0.05$ eV, whereas $Dq = 0.235$ eV, $Ds = 0.52$ eV, $Dt = 0.3$ eV were used for the low-spin ($S = 0$) configuration.

[66] In principle, depending on the temperature range, one should also include not only the chain susceptibility, i.e., the susceptibility of an endless antiferromagnetic chain [67], but also the boundary contribution arising from the staggered moment at the free ends of a chain segment [53,68]. However, as shown by Sirker *et al.* the generalized expression of χ, including all the terms mentioned above, reduces to the CW equation in the low-temperature limit [69]. Hence, we used the data below 10 K and fitted those to the CW equation to obtain the effective moment from which the spin state of Ni can be inferred.

[67] D. C. Johnston, R. K. Kremer, M. Troyer, X. Wang, A. Klümper, S. L. Bud'ko, A. F. Panchula, and P. C. Canfield, Phys. Rev. B **61**, 9558 (2000).

[68] S. Fujimoto and S. Eggert, Phys. Rev. Lett. **92**, 037206 (2004).

[69] J. Sirker, N. Laflorencie, S. Fujimoto, S. Eggert, and I. Affleck, Phys. Rev. Lett. **98**, 137205 (2007).

[70] T. Ami, M. K. Crawford, R. L. Harlow, Z. R. Wang, D. C. Johnston, Q. Huang, and R. W. Erwin, Phys. Rev. B **51**, 5994 (1995).

[71] K. Maiti, P. Mahadevan, and D. D. Sarma, Phys. Rev. B **59**, 12457 (1999).

[72] M. Rossi, H. Lu, A. Nag, D. Li, M. Osada, K. Lee, B. Y. Wang, S. Agrestini, M. Garcia-Fernandez, Y.-D. Chuang *et al.*, arXiv:2011.00595.

[73] J. H. Van Vleck, *The Theory of Electric and Magnetic Susceptibilities* (Clarendon, Oxford, 1932).

[74] P. Giannozzi, S. Baroni, N. Bonini, M. Calandra, R. Car, C. Cavazzoni, D. Ceresoli, G. L. Chiarotti, M. Cococcioni, I. Dabo *et al.*, J. Phys.: Condens. Matter **21**, 395502 (2009).

[75] J. P. Perdew, K. Burke, and M. Ernzerhof, Phys. Rev. Lett. **77**, 3865 (1996).

[76] D. Vanderbilt, Phys. Rev. B **41**, 7892 (1990).

[77] M. Cococcioni and S. de Gironcoli, Phys. Rev. B **71**, 035105 (2005).